Synthesis and Electrical Characterization of Magnetic Bilayer Graphene Intercalate

Namdong Kim,[†,§] Kwang S. Kim,[*,§] Naeyoung Jung,[‡] Louis Brus,[‡] and Philip Kim[*,†]

[†]Department of Physics and [‡]Department of Chemistry, Columbia University, New York 10027, United States
[§]Center for Superfunctional Materials, Department of Chemistry and Department of Physics, Pohang University of Science and Technology, Pohang 790-784, Korea

Ⓢ *Supporting Information*

ABSTRACT: We report synthesis and transport properties of the minimal graphite intercalation compound, a ferric chloride $(FeCl_3)_n$ island monolayer inside bilayer graphene. Chemical doping by the intercalant is simultaneously probed by micro-Raman spectroscopy and Hall measurements. Quantum oscillations of conductivity originate from microscopic domains of intercalated and unintercalated regions. A slight upturn in resistance related to magnetic transition is observed. Two-dimensional intercalation in bilayer graphene opens new possibilities to engineer two-dimensional properties of intercalates.

KEYWORDS: Bilayer graphene, intercalation, magnetic, $FeCl_3$, graphite intercalation compounds
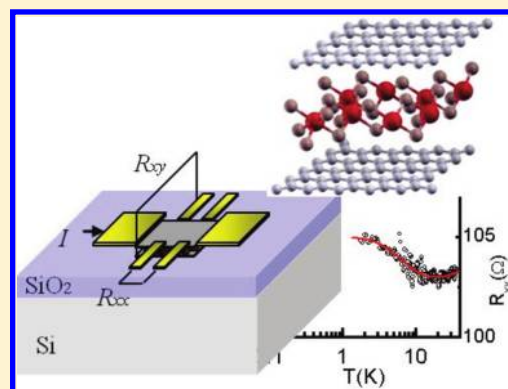
Graphite intercalation compounds (GICs)[1] with a periodic arrangement of an alternating sequence of intercalant and graphene layers exhibit a variety of exotic electronic properties ranging from superconductivity to magnetism. Recent advancement in graphene nanotechnology[2−6] opens a new avenue of creating few-layer graphene (FLG) intercalates. The surface boundary in FLG breaks the translational symmetry along the out-of-basal plane, yielding a new intercalation phase, not present in bulk GICs. FLG can be chemically modified by hybridization with other molecules via physical/chemical reactions into graphene derivative materials with widely different functionality.[7−9] Intercalation of FLG provides more robust chemical compound than a simple physical/chemical adsorption of molecules on the surface, since chemically inert and impermeable graphene layers protect the two-dimensional (2-D) intercalant layer in between to render further chemical protection.[10,11] In bulk forms of the GICs, a wide range of electronic properties, such as superconductivity,[12,13] magnetism,[14−21] and wide energy gap opening,[22] were discovered. Different chemical and physical properties are expected for FLG intercalation due to the increased surface-to-bulk ratio in the two-dimensional limit.[23] Magnetic or superconducting bilayer graphene (BLG) intercalation compounds are of particular interest, as these systems can be used to investigate the long-range ordered phenomena in two-dimensional systems. In this work, we choose $FeCl_3$ as the intercalant atomic layer, as the bulk $FeCl_3$ GIC exhibits stable ferromagnetic transition at temperature $T = 8.5$ K.[1,14,15]

$FeCl_3$ is intercalated into FLG samples deposited on a SiO_2/Si substrate in a saturated $FeCl_3$ vapor environment. We use in situ Raman spectroscopy to count the number of graphene layers,

probing atomic defects and identifying chemical doping of FLGs.[24,25] For most of the pristine FLGs, the G and 2D peaks are observed at ~1580 and ~2700 cm^{-1}, respectively, but with no significant D band at ~1350 cm^{-1}, which indicates high quality initial starting materials. Chemical reaction and device fabrication are carried out after this initial Raman spectroscopy characterization (Figure 1). After intercalation of $FeCl_3$ molecules, we find that the G peak, sensitive to charge doping,[10,25] exhibits a noticeable upshift, suggesting increased doping concentration. For single-layer graphene (SLG) samples, the G peak shows a strong upshift to ~1620 cm^{-1}, similar to bulk intercalation compounds[1,26] (Figure 1f). The corresponding charge doping estimated from this upshift is ~$5 \times 10^{13} cm^{-2}$, comparable to the highest doping achieved by ionic polymer electrolyte.[27] For bilayer graphene (BLG) samples, upshifts of the G peak beyond ~1620 cm^{-1} are observed (Figure 1f). This larger upshift of the G peak is accompanied by a change in the 2D band into a single broadened peak (Figure S2, Supporting Information), suggesting that each graphene layer in the bilayer sample behaves as an independent 2-D isolated monolayer.[11,24] The change of the 2D band in bilayer samples thus supports the proposition that $FeCl_3$ is intercalated between the graphene layers widening the separation between the layers that weaken the layer interaction. The similarity in the shift between SLG adsorption and BLG intercalation suggests that both cases contribute nearly equally to the increase in doping level. However,
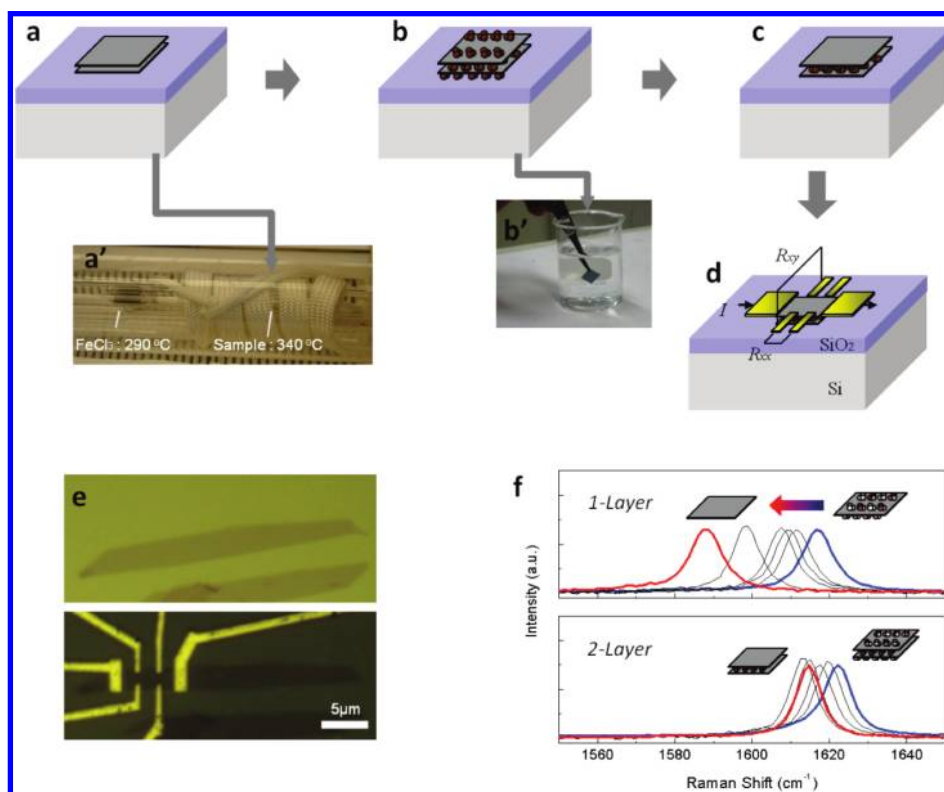
Figure 1. Fabrication of an intercalated bilayer graphene device. (a) Pristine bilayer graphene deposited on SiO_2/Si substrate. The graphene sample is put in a quartz tube with $FeCl_3$ powder. The sealed tube under vacuum is placed in the furnace (a′). (b) After reaction, molecules are adsorbed on and intercalated between graphenes. (c) Sufficient washing with acetone (b′) removes the adsorbed molecules from the surface, whereas the intercalated ones remain inside. (d) Deposition of electrodes using the standard fabrication technique. (e) Optical images before reaction (top) and after device fabrication (bottom). (f) Gradual downshifts of G peaks starting from ~1625 cm^{-1} (the position of reacted graphene initially in dry nitrogen gas without air exposure; blue), with repeated washings for single layer and bilayer. Each spectrum is taken in air after washing in acetone for 0, 0.16, 0.5, 1 (black), and 12 h (red).

the smaller upshift of the G peak in SLG indicates that adsorbed molecules dope graphene less effectively than intercalated ones.

We find that weakly binding molecules on the outer surface of samples are desorbed by vigorous rinsing. For the SLG samples, $FeCl_3$ molecules are adsorbed on the top surface of the SLG and possibly on the bottom interface between the graphene and SiO_2 surfaces. Adsorbed molecules can be simply removed from surfaces by washing with acetone (Figure 1f). The G peak shifts down continuously with increased washing according to the spectra recorded after each rinsing step. Doped SLG is gradually restored to "undoped" graphene (with the G peak position at ~1580 cm^{-1}) as adsorbed molecules are removed; however, the G peak of BLG does not shift back to the undoped value. The observed difference between SLG and BLG samples suggests the existence of stable $FeCl_3$-intercalated molecules protected by the top and bottom graphene layers. Although a weak solvent such as acetone does not remove the intercalated $FeCl_3$ molecules or a $(FeCl_3)_n$ island monolayer, more extensive rinsing in acetone or stronger solvents such as hydrocholoric acid eventually deintercalate the bilayer samples, splitting the G peak into a doublet of low-frequency G_L and high-frequency G_H (Supporting Information). Although $FeCl_3$ molecules are completely intercalated in graphene sheets initially, the sample undergoes slight deintercalation during device fabrication and likely finds a way toward its thermodynamically stable structure by formation of very small islands.[1] According to thick multilayer compounds,[1,26] the G peak splits into a doublet (G_L, G_H) due to two different

chemical environments of graphene sheets attributed to unintercalated and intercalated layers. As both layers in the intercalated bilayer graphene are exposed to similar chemical environments, the splitting in the G peak indicates microscopically inhomogeneous distribution of the intercalated area within the spot size of the Raman probe (~500 nm) due to partial deintercalation.

Exploiting the chemical stability of the intercalated bilayer graphene, we fabricate a Hall bar shaped device on the samples after surface-adsorbed molecules have been removed. After device fabrication which involves a lift-off process in acetone, a G peak shifts down to ~1615 cm^{-1} from ~1625 cm^{-1}, accompanied by splitting, while the 2D band is maintained a featureless single broad band (Figure S3, Supporting Information). Most of the adsorbed molecules are washed away during the device fabrication process, leaving the intercalated layer largely intact in the final bilayer device.

The structure of intercalated BLG is characterized by analyzing Shubnikov de Haas (SdH) oscillations in the magnetoresistance as a function of the magnetic field B perpendicular to the sample. The degenerately doped silicon substrate underneath 300 nm thick SiO_2 oxide serves as a back gate with gate voltage (V_g) to tune the additional carrier density n in the samples. When graphene is chemically doped, the charge neutrality point of graphene shifts in the positive direction far beyond the experimentally accessible back gate voltage range ($|V_g| \sim 100$ V), implying heavy p-doping ($n > 7 \times 10^{12}$ cm^{-2}). Temperature
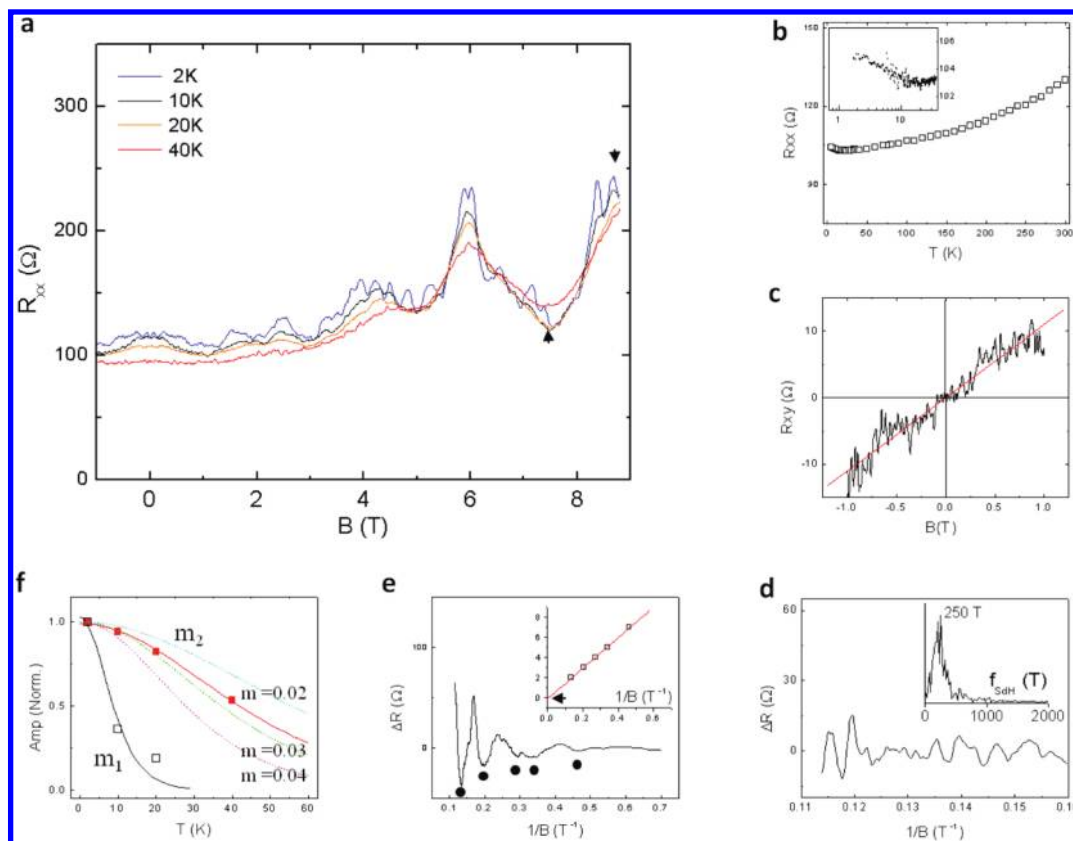
Figure 2. Transport measurements of an intercalated bilayer device. (a) Shubnikov-de Haas (SdH) oscillations seen in $R_{xx}(B)$ are recorded at temperatures 2, 10, 20, 40 K. (b) Temperature dependence of R_{xx} at $B = 0$ T. A weakly metallic R_{xx} exhibits a slight upturn around 15 K, shown in an inset with log-plot. (c) Hall resistance R_{xy} at $T = 1.6$ K. (d) The fast SdH oscillation at $T = 2$ K. The Fourier transform shown in an inset reveals a frequency $f_{SdH} \sim 250$ T. (e) The slow SdH oscillation at $T = 10$ K. Inset shows the fan diagram where the positions of minima (denoted by solid spots) in $R_{xx}(B)$ are plotted with the Landau level index. The slope of the linear fit corresponds to the frequency $f_{SdH} \sim 15$ T. The linear fit intercepts the origin (indicated by an arrow). (f) Temperature dependence of the SdH amplitudes at $B = 7.5$ and 8.5 T (indicated by arrows in a) yields the cyclotron masses m_2 for the slow oscillation and m_1 for the fast oscillation, respectively. The amplitudes are normalized to the values at the lowest temperature. Solid curves are the fits to the data points using the fitting formula (see the text). Dotted curves are the calculations done with different values of mass $m_2 = 0.02, 0.03, 0.04m_e$. The fitting of m_2 (red) lies between the calculations with $m_2 = 0.02, 0.03m_e$.

dependence of resistance (R_{xx}) of intercalated BLG shows a weakly metallic behavior down to $\sim$15 K. Below $\sim$15 K, there is a slight upturn with decreasing temperature (Figure 2b), the origin of which is not clear but is possibly related to magnetic transition. We note that similar anomalies in resistance have been reported in bulk magnetic GICs, where the abrupt change of resistance has been connected with its magnetic transition.[17,18]

To obtain the magnitude of carrier density, Hall voltage V_{xy} is measured at $T = 1.6$ K. Hall resistance changes up to $R_{xy} = V_{xy}/I = 10$ Ω at $B = 1$ T. Total carrier density is obtained from the Hall resistance, $n = B/eR_{xy} = 5 \times 10^{13}$ cm^{-2}. This hole carrier density agrees with the high upshift of Raman G peak and with our density functional theory (DFT) calculation ($\sim$0.01e per C atom). From the device geometry, the longitudinal resistivity of the sample is $\rho_{xx} \sim 100$ Ω with the sample mobility of $\mu = 1/ne\rho_{xx} \sim 0.12$ m^2/(V s) at the base temperature $T = 1.6$ K. This value is within the range of mobility of the potassium doped graphene.[28]

A simple estimation of the critical field $B_c = 1/\mu \sim 8$ T from the measured mobility suggests that one can expect to observe SdH oscillation, a quantum oscillation of resistivity due to the formation of Landau levels (LLs), in this sample within the experimentally accessible magnetic field. Figure 2a shows the

longitudinal resistance (R_{xx}) as a function of magnetic field B at different temperatures. At low temperatures, $R_{xx}(B)$ exhibits two distinct periodic oscillations, while at high temperatures only the low frequency oscillation survives. These two different types of magneto-oscillations arise from two different carrier densities n_1 and n_2 calculated using $n = g(e/h)f_{SdH}$, where f_{SdH} is the frequency of SdH oscillation in the $1/B$ plot and $g = 4$ to account for LL degeneracy considering spin and valley degrees of freedom.[3,4] The fast period of SdH is obtained from high pass filtering of the $T = 2$ K data in Figure 2a by subtracting the smooth background from R_{xx} and plotting the resulting ΔR as a function of $1/B$ (Figure 2d). By Fourier transformation of this fast SdH oscillation component (inset to Figure 2d), we obtain the fast SdH oscillation frequency, $f_{SdH} = 250$ T corresponding to carrier density $n_1 = 2.4 \times 10^{13}$ cm^{-2}, about half the total 2D sheet carrier density $n = 5 \times 10^{13}$ cm^{-2} from the Hall measurement. Given that intercalated bilayer samples have two identical layers with the same carriers degenerate in the Fermi surface, the SdH oscillations corresponding to $n_1 = n/2$ suggest that the two graphene layers are electrically decoupled by molecular intercalation.

While the faster SdH oscillations originate from the Dirac-like Fermi surface of the decoupled single-layer graphene, the slower
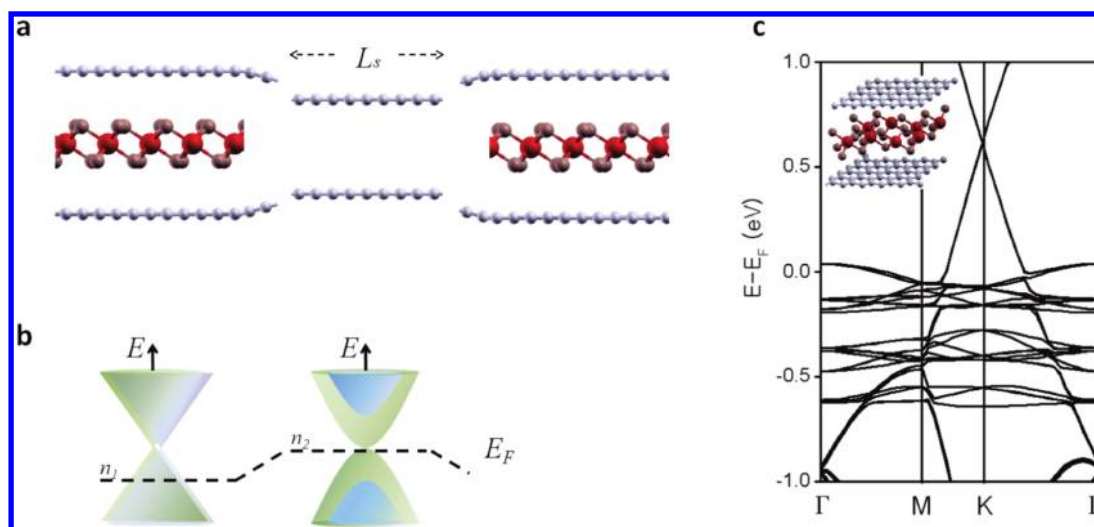
Figure 3. Atomic structural model. (a) Two different types of domains, intercalated (n_1) and unintercalated (n_2), are formed in bilayer graphene. Typical domain size (L_s) is much smaller than the beam spot size. (b) Band diagrams of two domains exhibit different electronic properties, especially chemical potential, carrier density, and band structures. (c) Band structure of intercalated bilayer graphene. DFT+U calculations predict the Fermi level shift of ~0.6 eV and charge transfer of ~0.01e per C atom. The flat bands below the Fermi level arise from Fe and Cl electrons. In an atomic model, carbon atoms are shown as gray spheres, iron atoms as red, and chlorine atoms as brown.

SdH oscillations suggest the existence of another Fermi surface. Since the faster SdH oscillations die out at higher temperatures, the slower component of SdH oscillations is readily extracted. Figure 2e shows the resistance change ΔR for the slow SdH oscillations after subtracting the smooth background from R_{xx} measured at 10 K. A regular oscillation in $1/B$ enables us to draw a Landau fan diagram, where the positions of minima in $R_{xx}(B)$ are plotted as a function of Landau level index (Figure 2e; inset). The slope of the linear fit is the slow SdH oscillation frequency f_{SdH} = 15 T, corresponding to the carrier density $n_2 = 1.4 \times 10^{12}$ cm^{-2}. The phase of this SdH oscillation is obtained from the y-intercept of the fan diagram. Typically, the SdH oscillation is described by $\Delta R \sim \cos[2\pi(f_{SdH}/B + 1/2 + \gamma)]$, where the phase of oscillation γ represents the Berry phase of the carrier.[3,4] For single-layer graphene, where carriers are Dirac fermions, nonzero π Berry's phase (i.e., $\gamma = \pm 1/2$) is expected. The linear fit of the fan diagram for the slow SdH oscillation intercepts the origin ($\gamma = 0$), indicating a trivial 2π multiple Berry phase. The lower carrier concentration with a trivial Berry phase associated with the second slow SdH oscillations, thus, suggests that some carriers belong to "coupled" bilayer graphene (i.e., nonintercalated bilayer).[5]

The observed SdH oscillation amplitude gradually dampens as temperature increases (Figure 2f). The oscillation amplitudes $A(T)$ at a particular magnetic field are expressed as $A(T) \sim u/\sinh(u)$, where $u = 2\pi^2 m_c k_B T/e\hbar B$[3,4] with cyclotron mass of charge carrier m_c. The obtained cyclotron masses are $m_1 = (0.15 \pm 0.03)\, m_e$ for high concentration n_1, and $m_2 = (0.026 \pm 0.004)\, m_e$ for low concentration n_2, where m_e is the bare electron mass. Here m_2 becomes close to ~0.03 m_e, the lower limit of electron mass in the pristine BLG.[29] Since the interlayer coupling γ_1 can be estimated from the relation, $m_2 = \gamma_1/2v_F^2$ at low doping level of the parabolic dispersion where v_F is the Fermi velocity,[5,30] this experimental observation suggests there is no appreciable band structure change in the pristine bilayer domains in our samples. For high doping of carriers n_1, the cyclotron mass m_1 reaches a high value of $m_1 = (\hbar/v_F)(\pi n_1)^{1/2} \sim 0.1 m_e$ by using monolayer dispersion.[1,3,4]

Since there are only two graphene layers in the intercalated BLG samples, two SdH oscillations associated with the intercalated decoupled bilayer (high carrier density) and the unintercalated coupled bilayer (low density) produce spatially inhomogeneous local charge distribution with structural variation (Figure 3a), below the limit of our AFM resolution. Island intercalation into small domain structures proposed here is in fact a common feature in bulk GICs, where the finite lateral size of typical domain structure is 10−50 nm with the domain boundary region less than 10 nm.[1,19−21] The island domain structure is taken into account as one of essential factors for understanding the magnetic long-range order in bulk GICs.[19−21]

To probe the inhomogeneous intercalation, we employ micro-Raman spectroscopy to map the local charge distribution in the device (Figure 4). Indeed, the Raman G peak in the device shows a distinct splitting into a low frequency G_L (~1585 cm^{-1}) and high frequency G_H (~1615 cm^{-1}) that match the intercalated and deintercalated domains, respectively, with variation in the relative intensities across the sample. Panels a−c of Figure 4 represent the relative intensities of IG_H to IG_L, and the positions of the higher shift G_H and the lower shift G_L at each spot, respectively, as indicative of signs of the degree of intercalation over the sample. In Figure 4d, each spectrum with two G peaks shows that two domains coexist in a small area of the lateral size of the probing beam spot. Considering that the spatial resolution limit of our micro-Raman spectroscopy is ~500 nm, we conclude that there are microscopic intercalated domains with size much smaller than 500 nm across the whole sample. A lower bound to the size of this microscopic domain L_s can be inferred from the magnetic length $l_B = (\hbar/eB)^{1/2}$ at the onset of the SdH oscillation $B \sim 3-5$ T, yielding $L_s > 10$ nm, in accordance with that observed in previous bulk intercalation compounds.[19−21]

In summary, by intercalating a magnetic $(FeCl_3)_n$ monolayer into BLG, we successfully measured highly doped Hall carrier density and cyclotron masses with the intercalants which form small islands during device fabrication.

Sample Reaction. FLG flakes are deposited by mechanical exfoliation onto highly doped Si wafer chips with 300 nm thick
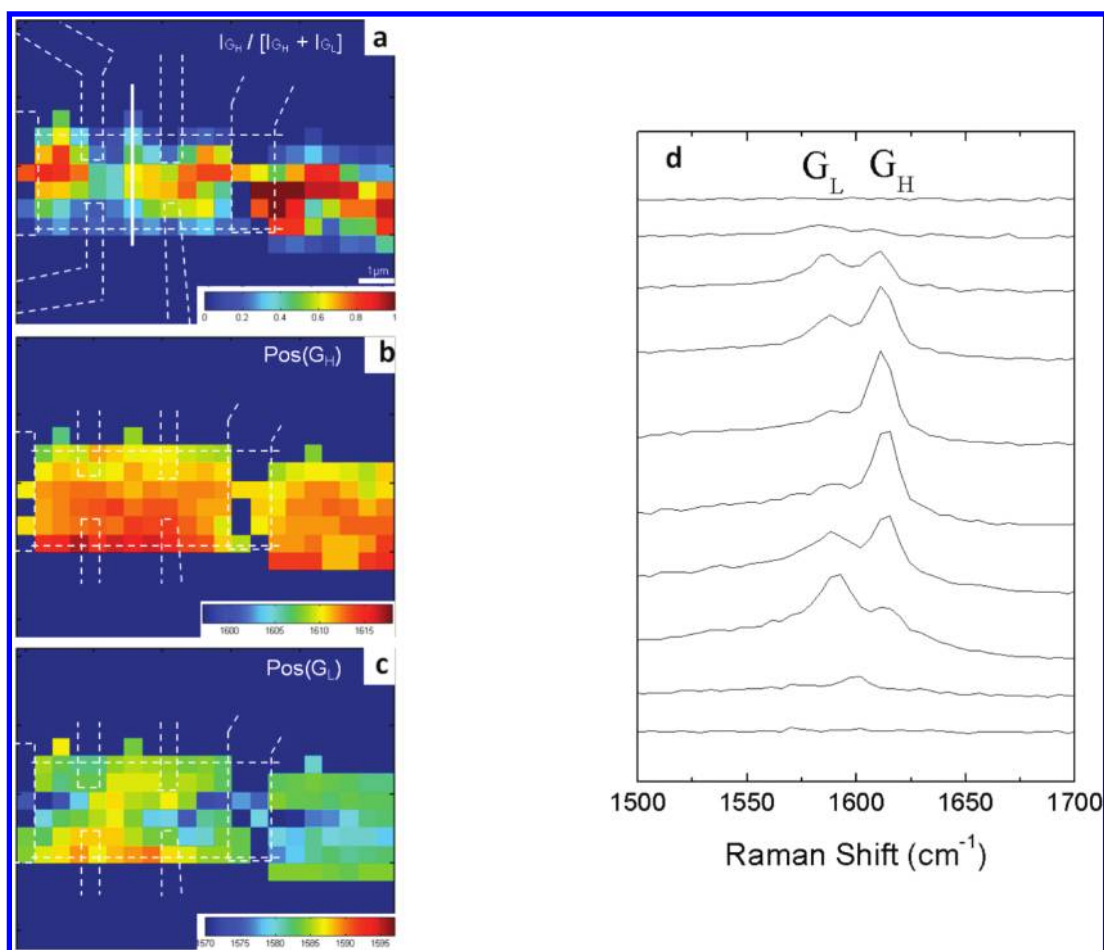
Figure 4. Micro-Raman measurements. (a−c) The relative intensities of IG_H to IG_L (a), the positions of the higher shift G_H (b) and the lower shift G_L (c) at each spot (500 nm) are mapped. These mappings indicate that small island intercalants are distributed over the sample. (d) Raman spectra taken at each spot along the white vertical line crossing the sample (a). Each G spectrum shows a doublet with a higher shift G_H and the lower shift G_L.

SiO_2/Si using adhesive tape.[2] Different graphene layers on the same SiO_2/Si substrate are examined through optical microscopy and Raman spectroscopy. For the vapor-phase reaction of ferric chloride ($FeCl_3$) and graphene, the two-zone method is employed.[1] The SiO_2/Si substrate containing a graphene sample is put in a quartz tube together with $FeCl_3$ powder, while avoiding contact between the two. The pressure in the quartz tube is decreased to $\sim 10^{-5}$ Torr (base pressure) over several hours after which it is sealed off under vacuum. The sample is then baked for a day in a furnace controlled at $T_g = 340$ °C for graphene and $T_i = 290$ °C for intercalant. To avoid sample degradation, moisture exposure is minimized. The reacted sample is removed in a glovebox filled with dry nitrogen gas, oxygen level <2 ppm and moisture level <1 ppm.

Device Fabrication. Metal contacts are severely destroyed in $FeCl_3$ vapor at high temperatures (~ 340 °C). Therefore, metal contacts (Cr (1 nm) /Au (30 nm)) are fabricated for transport measurement after the intercalation reaction. Intercalated samples are washed with acetone for ~ 6 h before device fabrication to remove adsorbed molecules. A Hall bar shaped device is fabricated in the standard electron beam lithography followed by the lift-off process in acetone. The synthesis and device fabrication of the $FeCl_3$-intercalated BLG were achieved in 2008.

Measurements and Calculation. We perform confocal backscattering Raman spectroscopy at 2 mW, 514 nm line of an argon laser irradiation. We measure transport properties using a standard lock-in technique with a current bias of $I = 100$ nA. We carry out DFT calculations using the VASP code with the GGA exchange correlation functional. The Coulomb interaction $U = 2.0$ eV was imposed on Cl atoms to correctly describe the charge distribution. The structure was optimized except for the interlayer distance, which was fixed to the value of bulk GIC, 0.94 nm, using the slab model with 5×5 (2×2) lateral periodicity of graphene ($FeCl_3$ layer).

■ ASSOCIATED CONTENT

⑤ Supporting Information. Raman shifts of few-layer graphene and bilayer graphene device through intercalation process. This material is available free of charge via the Internet at http://pubs.acs.org.

■ AUTHOR INFORMATION

Corresponding Author
*E-mail: K.S.K., kim@postech.ac.kr; P.K., pk2015@columbia.edu.

■ ACKNOWLEDGMENT

■ REFERENCES

(1) Dresselhaus, M. S.; Dresselhaus, G. *Adv. Phys.* **2002**, *51*, 1–186.

(2) Novoselov, K. S.; Geim, A. K.; Morozov, S. V.; Jiang, D.; Zhang, Y.; Dubonos, S. V.; Grigorieva, I. V.; Firsov, A. A. *Science* **2004**, *306*, 666–669.

(3) Novoselov, K. S.; Geim, A. K.; Morozov, S. V.; Jiang, D.; Katsnelson, M. I.; Grigorieva, I. V.; Dubonos, S. V.; Firsov, A. A. *Nature* **2005**, *438*, 197–200.

(4) Zhang, Y.; Tan, Y. W.; Stormer, H. L.; Kim, P. *Nature* **2005**, *438*, 201–204.

(5) Novoselov, K. S.; McCann, E.; Morozov, S. V.; Fal'ko, V. I.; Katsnelson, M. I.; Zeitler, U.; Jiang, D.; Schedin, F.; Geim, A. K. *Nat. Phys.* **2006**, *2*, 177–180.

(6) Kim, K. S.; Zhao, Y.; Jang, H.; Lee, S. Y.; Kim, J. M.; Kim, K.-S.; Ahn, J. H.; Kim, P.; Choi, J. Y.; Hong, B. H. *Nature* **2009**, *457*, 706–710.

(7) Stankovich, S.; Dikin, D. A.; Dommett, G. H. B.; Kohlhaas, K. M.; Zimney, E. J.; Stach, E. A.; Piner, R. D.; Nguyen, S. T.; Ruoff, R. S. *Nature* **2006**, *442*, 282–286.

(8) Li, X.; Zhang, G.; Bai, X.; Sun, X.; Wang, X.; Wang, E.; Dai, H. *Nat. Nanotechnol.* **2008**, *3*, 538–542.

(9) Tung, V. C.; Allen, M. J.; Yang, Y.; Kaner, R. B. *Nat. Nanotechnol.* **2009**, *4*, 25–29.

(10) Jung, N.; Kim, N.; Jockusch, S.; Turro, N. J.; Kim, P.; Brus, L. *Nano Lett.* **2009**, *9*, 4133–4137.

(11) Zhan, D.; Sun, L.; Ni, Z. H.; Liu, L.; Fan, X. F.; Wang, Y.; Yu, T.; Lam, Y. M.; Huang, W.; Shen, Z. X. *Adv. Funct. Mater.* **2010**, *20*, 3504–3509.

(12) Hannay, N. B.; Geballe, T. H.; Matthias, B. T.; Andres, K.; Schmidt, P.; MacNair, D. *Phys. Rev. Lett.* **1965**, *14*, 225–226.

(13) Weller, T. E.; Ellerby, M.; Saxena, S. S.; Smith, R. P.; Skipper, N. T. *Nat. Phys.* **2005**, *1*, 39–41.

(14) Karimov, Yu. S.; Zvarykina, A. V.; Novikov, Yu. N. *Sov. Phys. Solid State* **1972**, *13*, 2388.

(15) Ohhashi, K.; Tsujikawa, I. *J. Phys. Soc. Jpn.* **1974**, *36*, 422–430.

(16) Simon, Ch.; Batallan, F.; Rosenman, I.; Schweitzer, J.; Lauter, H.; Vangelisti, R. *Synth. Met.* **1983**, *8*, 53–59.

(17) Alaoui, M. K.; Piraux, L.; Bayot, V.; Issi, J. P.; Pernot, P.; Vangelisti, R. *Synth. Met.* **1989**, *34*, 537–542.

(18) Sugihara, K.; Yeh, N.-C.; Dresselhaus, M. S. *Phys. Rev. B* **1989**, *39*, 4577–4587.

(19) Dresselhaus, G.; Chen, S. T.; Szeto, K. Y. *Synth. Met.* **1985**, *12*, 433–438.

(20) Flandrois, S.; Hewat, A. W.; Hauw, C.; Bragg, R. H. *Synth. Met.* **1983**, *7*, 305–312.

(21) Speck, J. S.; Dresselhaus, M. S. *J. Phys.: Condens. Matter* **1990**, *2*, 6471–6489.

(22) Blinowski, J.; Rigaux, C. *J. Phys. (Paris)* **1980**, *41*, 667–676.

(23) Liu, L.; Ryu, S.; Tomasik, M. R.; Stolyarova, E.; Jung, N.; Hybertsen, M. S.; Steigerwald, M. L.; Brus, L.; Flynn, G. W. *Nano Lett.* **2008**, *8*, 1965–1970.

(24) Ferrari, A. C.; Meyer, J. C.; Scardaci, V.; Casiraghi, C.; Lazzeri, M.; Mauri, F.; Piscanec, S.; Jiang, D.; Novoselov, K. S.; Roth, S.; Geim, A. K. *Phys. Rev. Lett.* **2006**, *97*, No. 187401.

(25) Gupta, A.; Chen, G.; Joshi, P.; Tadigadapa, S.; Eklund, P. C. *Nano Lett.* **2006**, *6*, 2667–2673.

(26) Underhill, C.; Leung, S. Y.; Dresselhaus, G.; Dresselhaus, M. S. *Solid State Commun.* **1979**, *29*, 769–774.

(27) Das, A.; Pisana, S.; Chakraborty, B.; Piscanec, S.; Saha, S. K.; Waghmare, U. V.; Novoselov, K. S.; Krishnamurthy, H. R.; Geim, A. K.; Ferrari, A. C.; Sood, A. K. *Nat. Nanotechnol.* **2008**, *3*, 210–215.

(28) Chen, J.-H.; Jang, C.; Adam, S.; Fuhrer, M. S.; Williams, E. D.; Ishigami, M. *Nat. Phys.* **2008**, *4*, 377–381.

(29) Castro, E. V.; Novoselov, K. S.; Morozov, S. V.; Peres, N. M. R.; Lopes dos Santos, J. M. B.; Nilsson, J.; Guinea, F.; Geim, A. K.; Castro Neto, A. H. *Phys. Rev. Lett.* **2007**, *99*, No. 216802.

(30) Pereira, J. M.; Peeters, F. M.; Vasilopoulos, P. *Phys. Rev. B* **2007**, *76*, No. 115419.